Synthetic Metals 184 (2013) 52–60

Contents lists available at ScienceDirect

Synthetic Metals

journal homepage: www.elsevier.com/locate/synmet

A new route toward graphene nanosheet/polyaniline composites using a reactive surfactant as polyaniline precursor

Alejandro Vega-Rios, Flor Y. Rentería-Baltiérrez, Claudia A. Hernández-Escobar, E. Armando Zaragoza-Contreras *

Centro de Investigación en Materiales Avanzados, S.C., Miguel de Cervantes No. 120, Chihuahua, Chih., Mexico

ARTICLE INFO

Article history:
Received 22 May 2013
Received in revised form 25 August 2013
Accepted 13 September 2013

Keywords:
Nanocomposite
Graphene
Polyaniline
Surfmer

ABSTRACT

Graphene nanosheet/polyaniline nanocomposites were synthesized using anilium dodecylsulphate (DS-AN) first, as the surfactant to assist expanded graphite exfoliation, and then, as the monomer to synthesize conductive polyaniline. Based on this double functionality, DS-AN is classified as a reactive surfactant. I(G)/I(2D) ratios determined by Raman spectroscopy indicated nanosheet flakes in the range of 20 graphene layers. Similarly, electron microscopy gave also evidence of flakes consisting of layers of graphene in the same order. Concerning composite morphology, both electron microscopy and atomic force microscopy evidenced the formation of a polyaniline layer on the flakes, suggesting DS-AN polymerization occurred directly on the flake surface. Other composite characteristics such as specific surface area, determined by BET method, and electrical conductivity, determined by the four-probe method, showed inverse dependence with respect to polyaniline loading. By contrast, cyclic voltammetry showed, in all cases, increments of electroactivity as function of polyaniline loading.

1. Introduction

Graphite has a laminar structure, in which each graphite sheet is known as graphene, a two-dimensional lattice of carbon only a single atom thick. Graphene has emerged as one of the most important materials for current and future research, due to its outstanding electronic, optical, and mechanical properties [1,2]. On the search for the scale up production of graphene, the use of surfactants assisted by ultrasound has been widely reported. The reason for that is the hydrophobic nature of graphite; consequently, the use of surfactants is essential to produce stable aqueous dispersions of graphene. In addition, the economic and environmental advantages of handling aqueous dispersions are obvious. The products of this method are dispersions formed by mixtures of multilayered graphene (<10 layers). Surfactant function during graphite exfoliation are two: (a) lowering liquid–vapor interfacial energy of the solution to an optimal range that corresponds to the energy required to separate the sheets beyond the range of the van der Waals forces, and (b) adsorbing onto the graphene sheets, creating a repulsive surface preventing the reaggregation of the exfoliated sheets [3]. On this respect, several surfactants have been used; for example, Lotya et al. [4] took advantage of the methods that were reported to disperse carbon nanotubes in water and produced aqueous suspensions of multilayer graphene with the aid of sodium dodecylbenzenesulfonate. According to characterization, the product showed a low level of defects and anticipated that its properties could be improved by surfactant removal. Green and Hersam [5] produced stable aqueous graphene dispersions using bile salt sodium cholate as the stabilizer. To isolate graphene as function of their mean buoyant density (monodisperse thickness) ultracentrifugation was used. Fernández-Merino et al. [6] used series of non-ionic and ionic surfactants to produce stable graphene aqueous dispersions. Their results showed that non-ionic surfactants allow the production of dispersions with higher graphene contents. From these dispersions, paper-like films with significant electrical conductivity were obtained. Sim et al. [7] used sodium cholate and polyoxyethylene nonylphenol ether to obtain graphene aqueous dispersions. According to characterization, the dispersion consisted of a mixture of single, double, and few-layer graphene. Notley [3] used both non-ionic and ionic surfactants. His strategy, based on the continuous addition of surfactant that permitted keeping the liquid–vapor surface tension in the optimal range for the efficient graphene exfoliation, allowed producing highly concentrated graphene aqueous dispersions. Sun et al. [8] used the surfactant sodium taurodeoxycholate to produce stable aqueous dispersions with high content of graphene flakes with less than five layers. Graphene dispersions are potentially applicable in conductive films and in graphene based electrocatalysts. Smith et al. [9] produced aqueous dispersions of graphene using surfactant sodium cholate. They adopted sized exclusion chromatography to

* Corresponding author. Tel.: +52 614 439 4811; fax: +52 614 439 4811.
E-mail address: armando.zaragoza@cimav.edu.mx (E.A. Zaragoza-Contreras).

0379-6779/$ – see front matter © 2013 Elsevier B.V. All rights reserved.
http://dx.doi.org/10.1016/j.synthmet.2013.09.014

separate graphene dispersion into several fractions in accordance with their average lateral size. On the other hand, in the literature are found other studies that addressed the issue of a very broad manner [10–12].

However, surfactants are generally nonconductive, producing charge transfer blocking in the nanomaterial resulting in the deterioration of the graphene properties [13]. Therefore, before a subsequent application, further processing is required to remove the surfactant, which may be difficult by the strong surface interaction between surfactants and carbon materials. Besides, Brownson et al. [14] demonstrated that surfactants are a major contribution to the electrochemical performance of graphene electrodes and may be detrimental in electrochemical processes; that is, sometimes the electrochemical contribution of surfactants has been attributed to graphene itself.

Herein, we report the use of anilinium dodecylsulfate (DS-AN) as a reactive surfactant (surfmer); that is, on the one hand, it performs the common functions of a surfactant, and on the other hand, it is the monomer of polyaniline. It is possible to obtain graphene nanosheet/polyaniline nanocomposites without further requirement of critical cleaning or chemical reduction by using DS-AN, as after exfoliation it is submitted to an oxidative polymerization to obtain conductive polyaniline. We have reported recently the use of this novel concept of surfmer, *inverse surfmers*, in the synthesis of polystyrene/polyaniline core–shell composites via a two-step methodology: emulsion polymerization–oxidative polymerization [15] and the evaluation of electrical and electrochemical properties of these materials [16]. Consequently, the aim of this paper is to demonstrate the versatility of DS-AN as reactive surfactant in the synthesis of graphene nanosheet/polyaniline composites. First, DS-AN allowed the exfoliation of expanded graphite and subsequently, performed as the monomer of conducting polyaniline to produce graphene flakes covered by polyaniline. Consequently, this paper presents a new route using for the first time a molecule with the concept of DS-AN towards the synthesis of graphene nanosheet/polyaniline composites. However, we must mention that the concept of polymerizable anilinium salts is not new. Literature shows some reports on anilinium salts of dodecylbenzenesulfonate or dodecylsulfate. Sometimes the salts were isolated and polymerized [17–19] and some others were formed in situ during PAni polymerization [20–23]. In this report, we used microscopy techniques as essential tools to demonstrate the deposition of polyaniline on the graphene flake surface, as well as determinations of electroactivity and electrical conductivity to elucidate the effect of this new route on the composites properties, and to display possible practical applications.

2. Experimental

2.1. Materials

Expanded graphite (Grafoil grade GT-679, GrafTech International) was used as the source of graphite nanosheets. DS-AN was synthesized as described previously [15]. Ammonium persulfate (Aldrich Co.), the oxidizing agent, was recrystallized from a saturated aqueous solution at 50 °C.

2.2. Composite synthesis

In the first step, expanded graphite was treated as follows: 1.0 g of expanded graphite, DS-AN (variable concentration), and 150 cm^{-3} of distilled water were mixed in a glass vessel. The mixture was heated at 50 °C and left to mix for 24 h with gentle stirring. Afterwards, the mixture was left to cool at laboratory conditions and then put in refrigeration for 2 h. Finally, the mixture was sonicated using a sonic dismembrator (Model 505, Fisher Scientific) programmed to apply pulses with 100% of amplitude every 2 s for 60 min. The different studied mixtures are reported in Table 1.

Table 1
Formulations for the synthesis of graphene nanosheet/polyaniline composites.

Composite	Expanded graphite (g)	DS-AN wt% (mol)	APS (mol)
DS-5	1.0	5 (1.73×10^{-4})	1.73×10^{-4}
DS-10	1.0	10 (3.46×10^{-4})	3.46×10^{-4}
DS-20	1.0	20 (6.93×10^{-4})	6.93×10^{-4}

In the second step, DS-AN was submitted to an oxidative polymerization, by adding ammonium persulfate (APS) in molar ratio, APS:DS-AN, of 1.0:1.0. The polymerization was allowed for 48 h at −2 °C. After this time, the dark-green dispersion obtained was sonicated again under the same conditions as in step one. The solids were recovered by filtration and washed with distilled water to remove the co-products. Finally, the solids were redispersed in 200 cm^{-3} of distilled water by applying ultrasound for 2 min in a sonication bath. The final product was centrifuged at 4000 rpm for 15 min. The morphology and surface area of the suspended fraction was only considered for characterization. For characterization purposes, pure polyaniline was synthetized from DS-AN under the same conditions as in composite synthesis.

2.3. Characterization

Treated graphite and graphene nanosheet/polyaniline composites were characterized using a field emission scanning electron microscope (FE-SEM, JSM-7401F, JEOL Ltd.) and a field emission gun transmission electron microscope (JEM 2200FS, JEOL Ltd.). To prepare the samples, 0.1 cm^{-3} of graphite dispersion was redispersed in 20 cm^{-3} of distilled water. The diluted dispersion was sonicated for 5 min in a sonication bath. Then, a droplet of the dispersion was put on a holey-carbon–cooper grid.

Composite characterization was complimented using an atomic force microscope (MultiMode AFM, VEECO SPM) in the tapping mode, using a system 225 μm probe. Samples were prepared by dispersing 1 cm^{-3} of sobrenadant (after centrifugation) in 20 cm^{-3} of distilled water. Afterwards, a drop of dispersion was deposited on a fragment of silicon wafer and left to evaporate.

Expanded graphite and the exfoliated graphite were analyzed using a Micro-Raman spectrometer (LabRAM UV–VIS, Horiba Jobin-Yvon), at the excitation wavelength of 632.8 nm and 1800 mm^{-1} filter. The samples were prepared by casting a thin film of the aqueous dispersion onto Si/SiO_2 substrate.

Composites were also characterized by thermogravimetric analysis (TGA Q500, TA Instruments). Measurements were achieved using 10 mg of sample and heated from laboratory temperature to 950 °C, at a heating rate of 10 °C min^{-1}.

The conductivity of polyaniline and composites was determined by the four-probe technique. A homemade device was designed for this task. Probes of 10 mm (diameter) × 0.2 mm (width) were obtained by compression at laboratory conditions.

2.4. Cyclic voltammetry

Graphene nanosheet/polyaniline composites were characterized by cyclic voltammetry (CV) using a potentiostate analyzer (model 1260 plus 1287, Solartron). The software CorrView 2 was used to visualize the graphics. Electrochemical measurements were performed in a standard three-electrode cell at room temperature, using Pt wire (area = 0.03 cm^2) as the counter electrode, and Ag/AgCl/saturated KCl as the reference electrode. The working electrode was a polyethylene cylinder packed with carbon paste, with

a copper wire inserted through one end of the cylinder. The sample of dried composite was deposited on the opposite end to copper wire. A sulfuric acid (H_2SO_4) 2 mol dm^{-3} solution was used as the electrolyte. All cyclic voltammograms were recorded at a scan rate of 50 mV s^{-1} by sweeping the potential between −200 mV and +1000 mV against Ag/AgCl reference electrode.

3. Results and discussion

3.1. Morphology

In this study, DS-AN was used first, to exfoliate expanded graphite performing as a surfactant, and second, to obtain graphene nanosheet/polyaniline composites performing as the monomer of polyaniline. During exfoliation DS-AN performed in the same way as the common surfactants; that is, adsorbing on the surface of the graphite flakes creating a repulsive ionic layer avoiding reaggregation. Exfoliation, of course, was induced by ultrasound that is a fundamental factor in exfoliation [24]. Consequently, it is important to say that in this study all experiments were performed under the same sonication conditions. Micrographs of expanded graphite are portrayed in Fig. 1(a). As noted, expanded graphite consists of planar micrometric thick flakes formed, in turn, by a large number of graphene layers. On the other hand, after treatment, wrinkled flakes of graphene nanosheet of some few nanometers are obtained. High-resolution (HR) TEM, Fig. 1(b) showed that the flakes consist of a mixture of some few nanometric orderly arranged stacks that may be classified as few-layer-graphene (flakes with less than 10 individual layers of graphene). However, as the thickness of the flakes is highly variable we preferred to designate the material as graphene nanosheet.

To produce the graphene nanosheet/polyaniline composites, DS-AN was submitted to an oxidative polymerization using ammonium persulfate (APS) as the oxidizing agent. The products of this second stage were dark-green fluid dispersions, showing the presence of polyaniline in the conductive form (emeraldine base salt). Morphology of pure polyaniline and graphene nanosheet/polyaniline composites was observed by STEM, Fig. 2(a–d). As observed, PAni particles obtained from the chemical polymerization of DS-AN are in the range of 10–30 nm, lots of them of elongated shape (nanofibers). In the case of the composites, the exfoliation gained in the first step was kept; that is, flake reagglomeration was not evident. Such finding was attributed to the strong interaction between DS-AN and the flake surface. Figure 1S (see Supplementary Material) illustrates DS-AN molecular structure, as noted, the molecule contains the typical constituents of conventional anionic surfactants; that is, a hydrophobic hydrocarbon chain (dodecyl radical) and a hydrophilic head group with the anilinium group as the counterion. DS-AN critical micellar concentration and Krafft temperature have been reported previously [15]. This way, after treatment, the flakes were covered by DS-AN. Thanks to that, it is very probable that the thin PAni layer formed are the result of direct DS-AN polymerization on the flakes surface, and not the mere deposition of PAni particles produced in the aqueous phase.

To deepen in the composites microstructure, HRTEM and atomic force microscopy (AFM) were performed. Fig. 3(a) portraits images of the composite synthesized with 10 wt% DS-AN and of a clean graphene flake, Fig. 3(b). As observed, the composite surface shows roughness associated with PAni deposition. Whereas the clean flake surface shows the carbon atomic network typical of graphene. Complementarily, for tell apart between graphene and PAni, phase-contrast analysis was performed, Fig. 4. First, the contrast between the PAni particles (lighter phase) and the grid carbon support (darker phase) is clearly noted; the optical difference between materials is related to material density. In the case of the composites, the presence of PAni (lighter phase) increased with DS-AN initial loading that indicates higher PAni content. Besides, it is evident that PAni is deposited in the form of nanometric particles; that is, definitely PAni is not forming a continuous film. Zooming on one flake exhibited clearly the presence of the PAni layer as shown by STEM and HRTEM. As a result, flake thickness in the range of 1 nm can be deduced; that is, an important population of graphene flakes can be classified as single-layer graphene. Finally, Fig. 3(a,b) gave clear evidence of the particulate nature of PAni; it is also noted that PAni is apparently deposited as layers or strata, since a sublayer of PAni particles, apparently of smaller size, is observed in a first plane; whereas in a superior plane a layer of larger PAni particles is observed. On the other hand, AFM images of the composite synthesized with 10 wt% DS-AN, are portrayed in Fig. 5. As noted, fragments of different size and shape are present. Thickness of ca. 3.5 nm was determined from series of flakes with similar texture, as seen in Fig. 5(b).

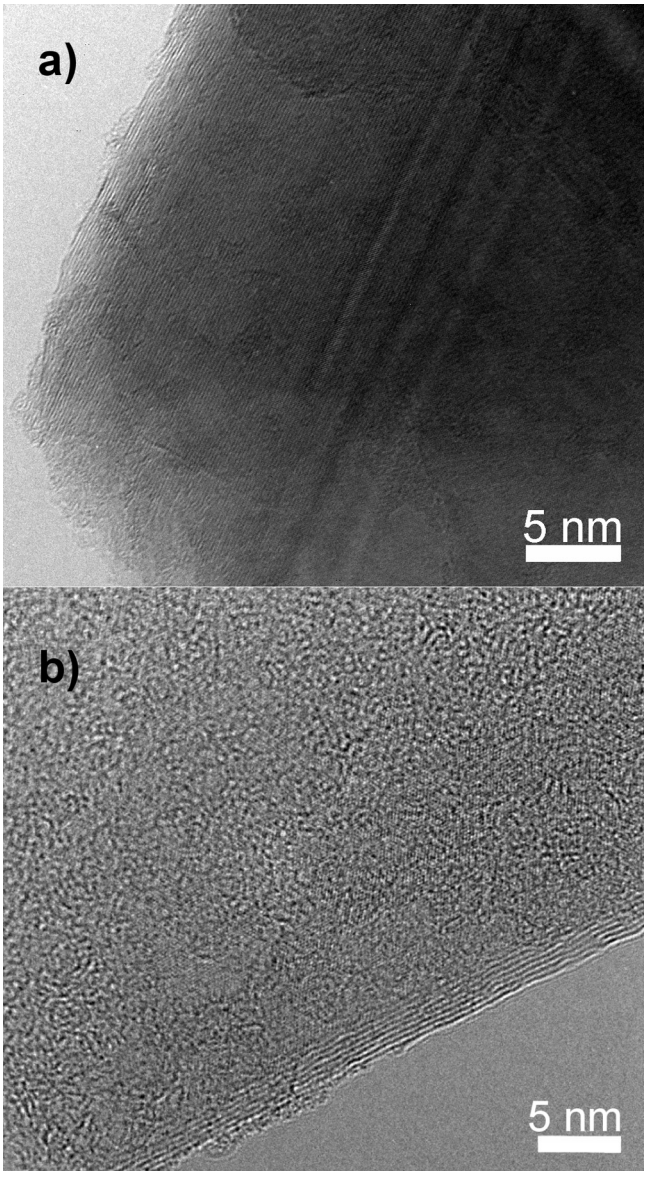

Fig. 1. Micrographs of high resolution (HR) TEM. (a) Expanded graphite, (b) treated graphite (graphene nanosheet) with less than 10 graphene.

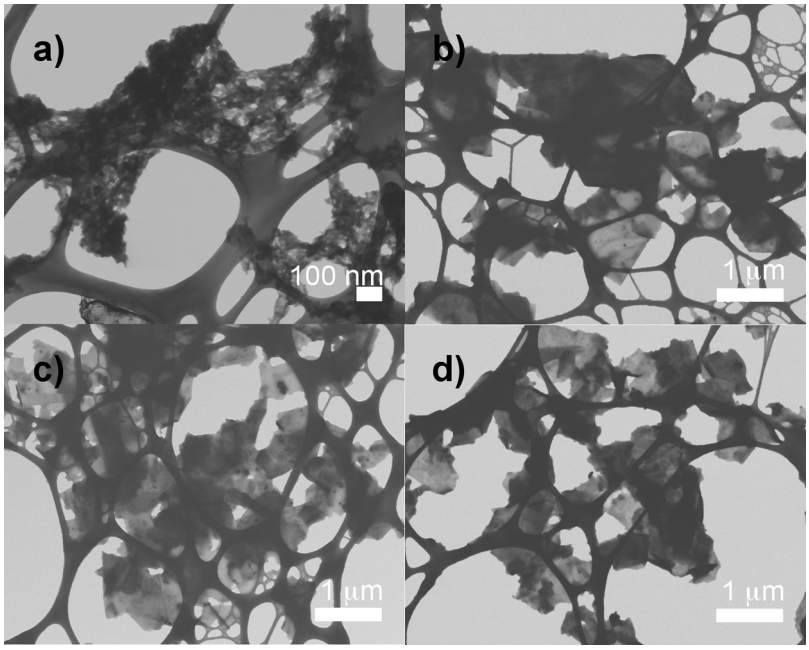

Fig. 2. FE–SEM images. (a) PAni, and (b–d) composites synthesized with 5, 10, 20 wt% DS-AN, respectively.

3.2. Exfoliation

Fig. 6 shows Raman spectra of expanded graphite and composites synthesized with 5, 10 and 20 wt% DS-AN. In all spectra the composites show the three typical peaks of graphite at 1350, 1600, and 2700 cm^{-1}. These bands correspond, respectively, to D, G, and 2D bands. The D peak is due to A_{1g} mode breathing vibrations of six-membered sp^2 carbon rings, which are absent in defect-free graphene. The G band corresponds to zone center phonons of E_{2g} symmetry. The significant change in intensity of the 2D peak of the treated graphite compared to the same peak in expanded graphite, were considered an evidence of graphite exfoliation [25]. An important factor is the ratio between the intensity of G and 2D line, I(G)/I(2D). The increase in this ratio is related to the increment in the number of graphene layers. Concerning this, our results indicated a I(G)/I(2D) ratio of 1.2, 1.25 and 1.4 for the composites with DS-AN 5%, 10% and 20%, respectively, suggesting graphene layers in the range of 20 [26].

The evolution of the 2D band as a function of the number of graphene layers has been pointed out by several authors, where a further increase of the number of layers leads to a significant decrease of the relative intensity of the 2D peak [27]. Graphene has a single, sharp 2D peak, roughly four times more intense than the G peak [28]. The 2D peak in Fig. 6 shows the evolution of the peak 2D regarding DS-AN concentration indicating, according to the shape of the peak, graphene layers in the order of 10 or higher [25]. Jorio et al. [29] also gave a detailed description of how the multipeak structure of the 2D band observed for a stacking of two or more graphene layers is related to the differences between graphene samples with different thicknesses. In addition to the differences in the 2D band, the intensity of the G band increases almost linearly as the graphene thickness increases, this can be readily understood as more carbon atoms are detected for multi-layer graphene. According to these results, we can say that the expanded graphite was successfully exfoliated by DS-AN and assistance of ultrasound, and that polyaniline polymerized onto the graphene nanosheet avoided restacking. Complementarily, the exfoliation of expanded graphite in the composites was studied by X-ray diffraction, where the 002 peak, characteristic of graphite, decreased in intensity and width, which has been reported as evidence of exfoliation (see Figure 2S and Table 1S, Supplementary material section) [30,31].

3.3. Surface area

The specific surface area of 156.96 $m^2 g^{-1}$ was determined for the graphene nanosheet by BET. The larger surface area shown with respect to the expanded graphite was attributed to exfoliation. However, this value decreased after DS-AN polymerization; that is, as the nanographite flakes were coated by a layer of PAni the surface porosity was blocked, reducing the surface area as a consequence. Nevertheless, the surface area of the composites was much larger than that of the pure PAni. This enhancement was attributed to graphite exfoliation since in the composites the PAni is as a coating and in the pure form as an agglomeration of particles. The detailed surface areas are listed in Table 2. Literature reports, for instance, specific surface areas of pristine graphene and graphene/PAni composite, respectively, of 186.6 $m^2 g^{-1}$ and 40.5 $m^2 g^{-1}$ [32]. In this case, graphene surface area decreased also with PAni coating. Concerning other similar systems, the specific surface area for CNT composites with 66 wt% PAni was found to be 54.3 $m^2 g^{-1}$ [33].

3.4. Thermal stability and composite composition

Fig. 7 shows TGA traces of expanded graphite, graphene nanosheet, polyaniline, and the composites. As observed, graphene nanosheet was stable up to 637 °C to then degrade continuously

Table 2
Specific surface area of graphene nanosheet/polyaniline composites and conversion of DS-AN to polyaniline determined, respectively, by BET and TGA.

Sample	Specific surface area ($m^2 g^{-1}$)	PAni (wt%)	Conversion (%)
Expanded graphite	93.29	–	–
Nanographite	156.96	–	–
PAni	19.67	–	–
DS-5	123.28	3.0	60.4
DS-10	111.09	5.1	50.9
DS-20	98.73	11.3	56.4

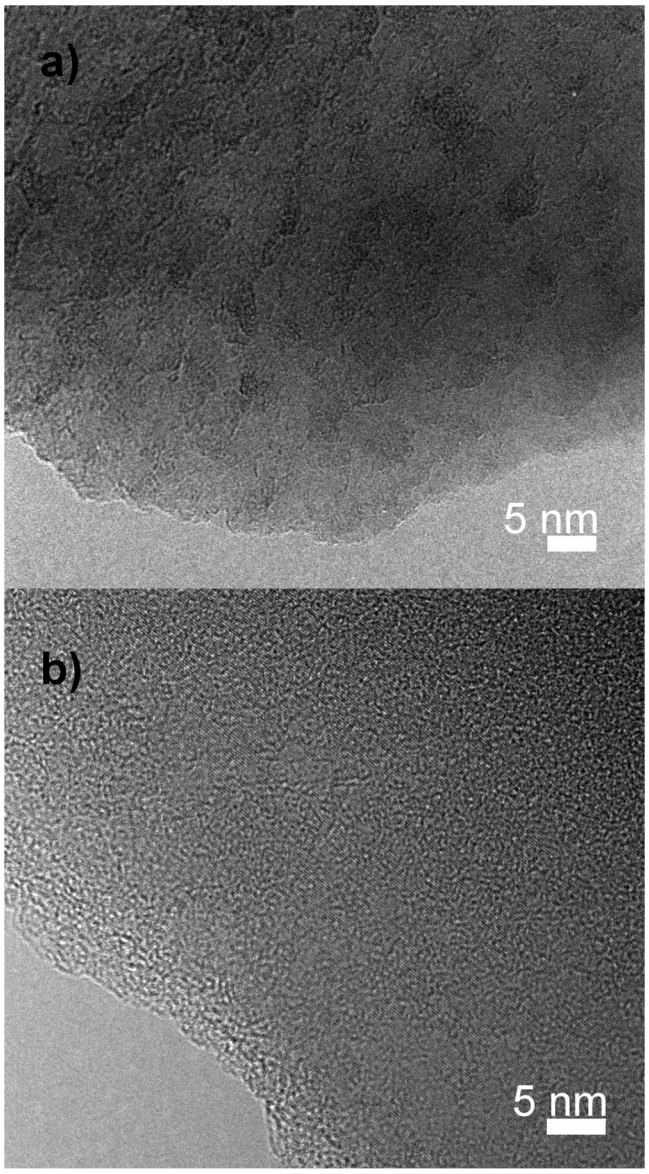

Fig. 3. HRTEM images. (a) 10 wt% DS-AN, (b) clean graphene flake.

until 800 °C. This behavior has been attributed to carbon oxidation to carbon dioxide [34,35]. On the other hand, in the case of the expanded graphite, no weight loss is observed until 706 °C; that is, the expanded graphite is 70 °C more thermally stable than the nanographite. Such difference has been explained in terms of; i.e., decreased van der Waals interaction [34]. Concerning polyaniline, a mass loss at ca. 230 °C is observed, which was associated to degradation of the doping agent. Subsequently, another transition at ca. 350 °C is observed; this transition was attributed to the decomposition of the polyaniline backbone [36,37]. Finally, the composites showed a progressive mass decrement with increment in PAni content. It is also noticed that the weight loss curve of composites appears above that of pure PAni, showing the enhanced thermal stability of the composites. This can be ascribed to the barrier character of graphene nanosheet for the degradation of PAni [38].

Conversion of DS-AN to polyaniline, determined from TGA data, is reported in Table 2. As noted, the yield of the polymerization was between 50 and 60%, without evident tendency with respect to DS-AN loading. Moderated conversion was attributed to the strong interaction between DS-AN and the flake, which restricted apparently the movement of the molecules of DS-AN during polymerization.

3.5. Composite electrical conductivity

Usually, polymer/graphene composites present improved properties which led to a wide variety of applications; i.e., sensors, catalysis, or energy storage [39]. In a previous report, the polystyrene/polyaniline core–shell composites using DS-AN as the polyaniline precursor, exhibited conductivity in the range 6.42×10^{-6} to 0.01 S cm^{-1} at PAni loadings, respectively, of 3.3 and 26.7 wt% [16]. Composite electrical conductivity, based on the PAni content determined by TGA, is reported in Table 3. As observed, electrical conductivity of expanded graphite and graphene nanosheet are the same, which is not strange considering that both materials were compressed to prepare the samples for characterization. In the case of the composites, conductivity exhibited progressive decrement with the increase of polyaniline loading. This result confirmed that PAni is covering the flakes. If we consider that polyaniline (semiconductor) is less conductive than graphene nanosheet, conductivity depression with the increment of PAni is a logical result, suggesting also that is increasingly thicker the polyaniline layer. It is worth saying that the conductivities reported in literature for expanded graphite and PAni, are in the same order of the values showed here [40–42].

In the case of expanded graphite/polyaniline composites reported by Xiang et al. [40], conductivities of pure expanded graphite and pure PAni were, respectively, 110.50 and 0.17 S cm^{-1}, whereas conductivities of the composites increased along with the increase of expanded graphite content. In this case, the conduction mechanism of expanded graphite includes two respects: the electron directional movement in the expanded graphite layers and the electron transition between the layers. On the one hand, the PAni conjugated chains offer lots of conductive paths on the surface of graphite layers, which activates more electrons to participate in the directional movement. On the other hand, the embedding of PAni particles onto expanded graphite layers may cause some interactions between PAni chains and graphite layers. The synergistic effect of these two parts leads to the notable increase of the conductivity of graphite/polyaniline composites [43,44]. Our results showed that conductivity decreased with PAni content; however, if we consider results inversely, we see that, in fact, the conductivity improved with the content of graphene nanosheet. Therefore,

Table 3
Four-probe electrical conductivity of expanded graphite, graphene nanosheet, PAni, and graphene nanosheet/PAni composites.

Sample	t (cm)	R (Ohm)	t/s	ρ (Ohm cm)	σ (S cm^{-1})
Expanded graphite	0.1236	0.005	0.4696	0.0028	357.01
(Treated graphite)	0.1236	0.005	0.4696	0.0028	357.01
PAni	0.1236	12.323	0.4696	6.9033	0.14
CDS-3.0	0.1236	0.009	0.4696	0.0050	198.34
CDS-5.1	0.1236	0.010	0.4696	0.0056	178.50
CDS-11.3	0.1236	0.011	0.4696	0.0061	162.28

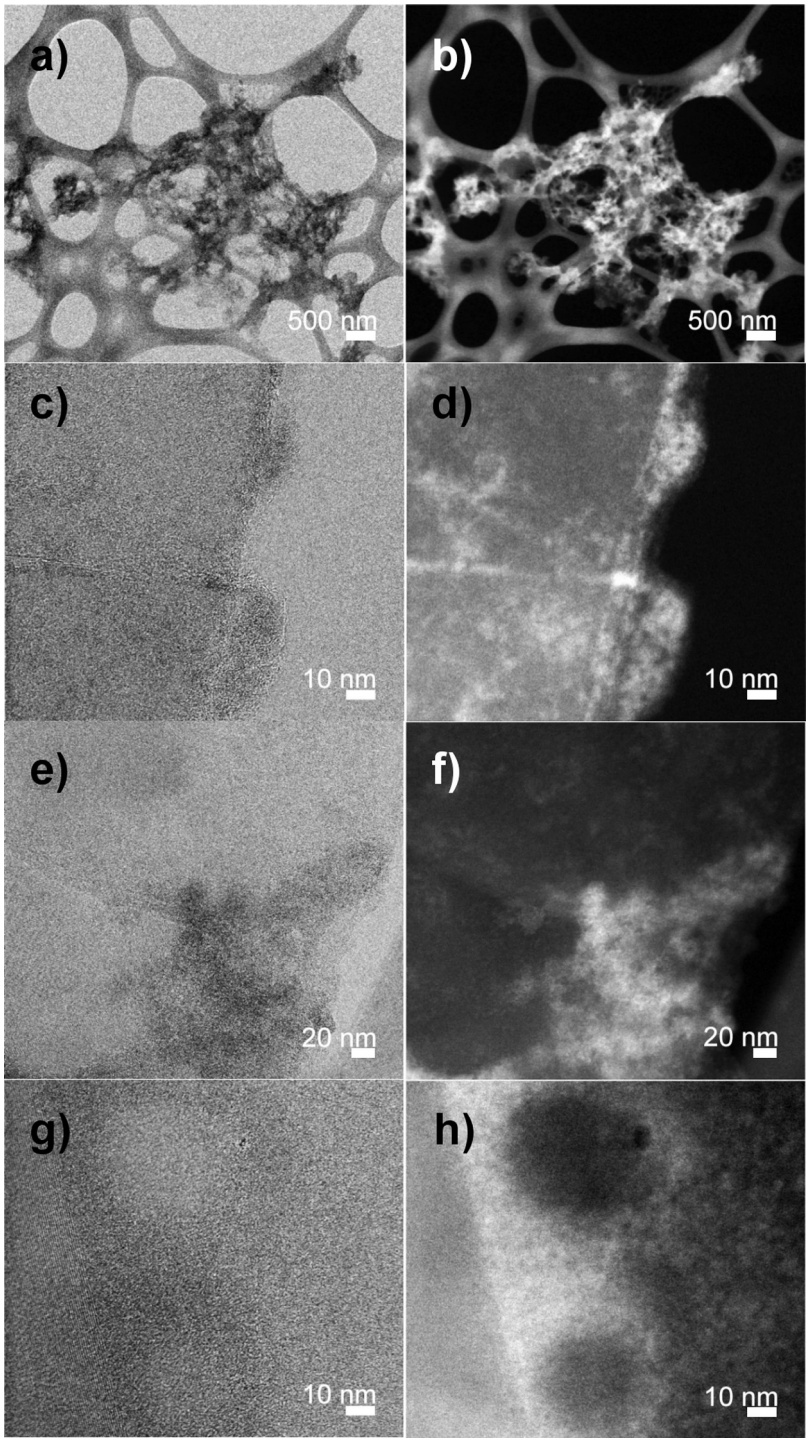

Fig. 4. Phase-contrast analysis. (a) PAni, (c, e, g) composites synthesized with 5, 10, 20 wt% PAni, respectively and (b, d, f, h) phase-contrast PAni and each of the compositions.

this interpretation can be appropriately applied to describe the observed behavior. In the case of composites of polyaniline with nanotubes or graphene, similar interpretation has been given [45,46].

Four-probe conductivity, in the presence of conventional surfactants (SDS or SDBS) has been reported; i.e., in the case of single-walled nanotubes (SWCNT) the conductivity of PAni/SWCNT/SDBS nanocomposite increased, respectively, from 8.58 to 18.20 S cm^{-1} at 0.3 to 3.8 wt% SWNTs. On the other hand, nanocomposites prepared using SDS exhibited low conductivity up to 0.6 wt% SWCNT. The conductivity values are in fact lower than PAni/SDS. This low conductivity was attributed to lower effective doping of PAni/SWCNT in the presence of SDS. On further addition of SWCNT the conductivity started to increase but always, remained lower compared to SDBS counterparts. The difference in the conductivity was attributed to the complex interactions between PAni/surfactant/SWCNT [47].

3.6. Composite electroactivity

Carbon materials have been used for years as electrodes, because of their properties such as high conductivity, wide potential

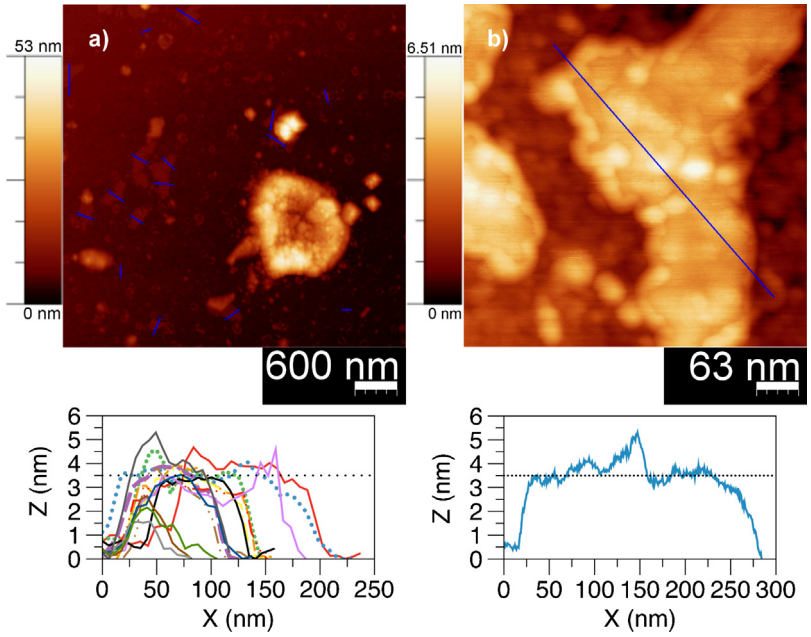

Fig. 5. AFM images of the composite synthesized with 10 wt% DS-AN. (a) Image 3 × 3 μm, (b) amplification.

window, and electrocatalytic activity for various redox reactions [48]. Voltammograms of the composites, in 2 M H_2SO_4, at a scan rate of 50 mV s^{-1} are shown in Fig. 8. As noted, in the potential region, between −200 and 1000 mV, both the response of current density and integrated charge increase as function of PAni content, demonstrating, in all cases, electroactivity. Clear redox peak of PAni is observed in all plots. During cycling, the positive range was swept from the half-doped state, called emeraldine, to fully doped state, called pernigraniline. On the other hand, the negative range was swept from half-doped state to fully dedoped state, called leucoemeraldine. Both leucoemaraldine and pernigraniline states are non-conducting in nature, and offer high resistance. At a high voltage of the cell, PAni does not have sufficient ion exchange sites to get doped. Hence, there is a decrease in current for the supercapacitor above 0.6 V. According to literature, voltammetric response of polyaniline in acidic medium has two couplings redox potential in the range of −0.2 V < V < 1 V [49]. In the potential range between −0.2 and 1 V, the compounds show a redox couple that is manifested as two voltammetric peaks. These peaks are not symmetric with respect to shape or position on the potentials axis. The cathodic peak is always wider and appears at inferior potential values.

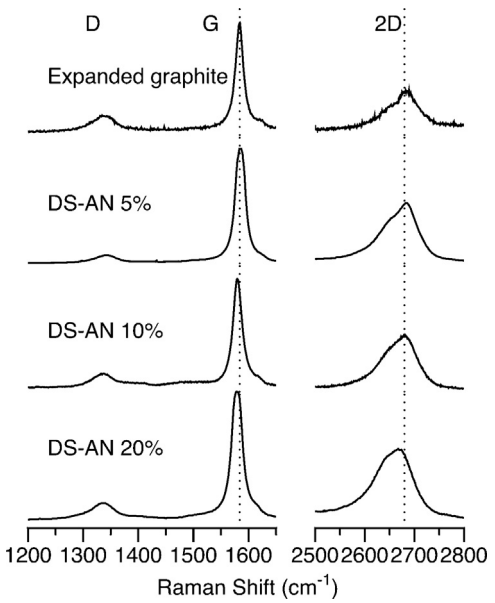

Fig. 6. Raman spectroscopy. (a) Expanded graphite and (b) treated graphite (graphene nanosheet).

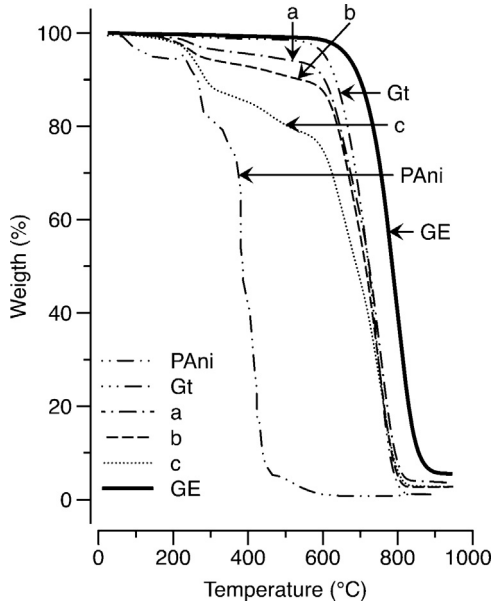

Fig. 7. TGA traces of expanded graphite (GE), treated graphite (Gt), PAni, and (a–c) composites with 3, 5.1, 11.3 wt% PAni, respectively.

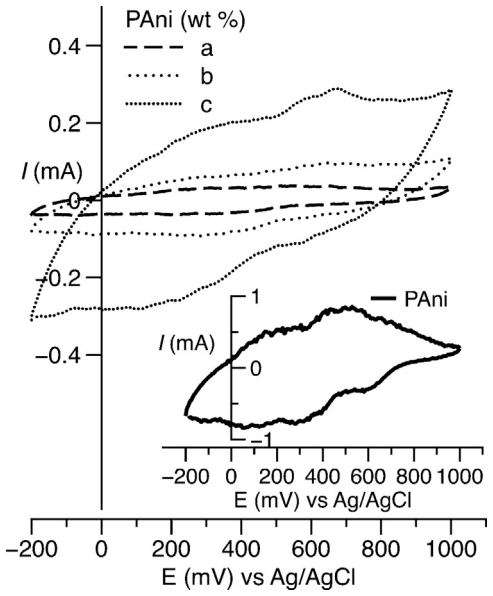

Fig. 8. Voltammograms of graphene nanosheet/PAni composites. (a) 3, (b) 5.1, (c) 11.3 wt% PAni.

4. Conclusion

We have demonstrated the application of anilinium dodecylsulphate (DS-AN) as a new route toward the production of graphene nanosheet/polyaniline composites, taking advantage of the double functionality surfactant-monomer of DS-AN. Results showed that both surface area and electrical conductivity are function of polyaniline loading, which confirmed that the graphene flakes are covered by a polyaniline layer. DS-AN polymerization occurred directly on the graphene flake surface because of the strong interaction between both materials. Cyclic voltammetry showed a similar behavior to that reported in literature, with increments in electroactivity with respect to PAni loading. Finally, it can be mentioned that based on the composite properties, applications in sensors design or supercapacitors are evident.

Acknowledgments

We wish to thank the National Council for Science and Technology of Mexico (CONACYT) for the grant awarded to Flor Y. Rentería-Baltiérrez. We also wish to thank to the Laboratorio Nacional de Nanotecnología, and to Daniel Lardizabal, Wilber Antunez, Carlos Ornelas, and Pedro Pizá for their helpful collaboration during this research.

Appendix A. Supplementary data

Supplementary data associated with this article can be found, in the online version, at http://dx.doi.org/10.1016/j.synthmet.2013.09.014.

References

[1] A.K. Geim, K.S. Novoselov, The rise of graphene, Nat. Mater. 6 (2007) 183–191.
[2] C. Lee, X. Wei, J.W. Kysar, J. Hone, Measurement of the elastic properties and intrinsic strength of monolayer graphene, Science 321 (2008) 385–388.
[3] S.M. Notley, Highly concentrated aqueous suspensions of graphene through ultrasonic exfoliation with continuous surfactant addition, Langmuir 28 (2012) 14110–14113.
[4] M. Lotya, Y. Hernandez, P.J. King, R.J. Smith, V. Nicolosi, L.S. Karlsson, et al., Liquid phase production of graphene by exfoliation of graphite in surfactant/water solutions, J. Am. Chem. Soc. 131 (2009) 3611–3620.
[5] A.A. Green, M.C. Hersam, Solution phase production of graphene with controlled thickness via density differentiation, Nano Lett. 9 (2009) 4031–4036.
[6] L. Guardia, M.J. Fernández-Merino, J.I. Paredes, P. Solís-Fernández, S. Villar-Rodil, A. Martínez-Alonso, et al., High-throughput production of pristine graphene in an aqueous dispersion assisted by non-ionic surfactants, Carbon 49 (2011) 1653–1662.
[7] Y. Sim, J. Park, Y.J. Kim, M.-J. Seong, S. Hong, Synthesis of graphene layers using graphite dispersion in aqueous surfactant solutions, J. Korean Phys. Soc. 58 (2011) 938.
[8] Z. Sun, J. Masa, Z. Liu, W. Schuhmann, M. Muhler, Highly concentrated aqueous dispersions of graphene exfoliated by sodium taurodeoxycholate: dispersion behavior and potential application as a catalyst support for the oxygen-reduction reaction, Chem. Eur. J. 18 (2012) 6972–6978.
[9] R.J. Smith, P.J. King, C. Wirtz, G.S. Duesberg, J.N. Coleman, Lateral size selection of surfactant-stabilised graphene flakes using size exclusion chromatography, Chem. Phys. Lett. 531 (2012) 169–172.
[10] S. Lin, C.-J. Shih, M.S. Strano, D. Blankschtein, Molecular insights into the surface morphology, layering structure, and aggregation kinetics of surfactant-stabilized graphene dispersions, J. Am. Chem. Soc. 133 (2011) 12810–12823.
[11] E.E. Tkalya, M. Ghislandi, G. de With, C.E. Koning, The use of surfactants for dispersing carbon nanotubes and graphene to make conductive nanocomposites, Curr. Opin. Colloid Interface Sci. 17 (2012) 225–232.
[12] E. Coşkun, E.A. Zaragoza-Contreras, H.J. Salavagione, Synthesis of sulfonated graphene/polyaniline composites with improved electroactivity, Carbon 50 (2012) 2235–2243.
[13] F.J. Tölle, M. Fabritius, R. Mülhaupt, Emulsifier-free graphene dispersions with high graphene content for printed electronics and freestanding graphene films, Adv. Funct. Mater. 22 (2012) 1136–1144.
[14] D.A.C. Brownson, J.P. Metters, D.K. Kampouris, C.E. Banks, Graphene electrochemistry: surfactants inherent to graphene can dramatically effect electrochemical processes, Electroanalysis 23 (2011) 894–899.
[15] E.A. Zaragoza-Contreras, M. Stockton-Leal, C.A. Hernández-Escobar, Y. Hoshina, J.F. Guzmán-Lozano, T. Kobayashi, Synthesis of core–shell composites using an inverse surfmer, J.Colloid Interface Sci. 377 (2012) 231–236.
[16] A. Vega-Rios, C.A. Hernández-Escobar, E.A. Zaragoza-Contreras, T. Kobayashi, Electrical and electrochemical properties of polystyrene/polyaniline core–shell materials prepared with the use of a reactive surfactant as the polyaniline shell precursor, Synth. Met. 167 (2013) 64–71.
[17] N. Kuramoto, A. Tomita, Aqueous polyaniline suspensions: chemical oxidative polymerization of dodecylbenzene-sulfonic acid aniline salt, Polymer 38 (1997) 3055–3058.
[18] Y. Haba, E. Segal, M. Narkis, G.I. Titelman, A. Siegmann, Polyaniline-DBSA/polymer blends prepared via aqueous dispersions, Synth. Met. 110 (2000) 189–193.
[19] V. Rumbau, J.a. Pomposo, J.a. Alduncin, H. Grande, D. Mecerreyes, E. Ochoteco, A new bifunctional template for the enzymatic synthesis of conducting polyaniline, Enzyme Microb. Technol. 40 (2007) 1412–1421.
[20] W. Yin, E. Ruckenstein, Soluble polyaniline co-doped with dodecyl benzene sulfonic acid and hydrochloric acid, Synth. Met. 108 (2000) 39–46.
[21] D. Tsotcheva, T. Tsanov, L. Terlemezyan, S. Vassilev, Structural investigations of polyaniline prepared in the presence of dodecylbenzenesulfonic acid, J. Therm. Anal. 63 (2001) 133–141.
[22] L. Yu, J. Lee, K. Shin, C. Park, R. Holze, Preparation of aqueous polyaniline dispersions by micellar-aided polymerization, J. Appl. Polym. Sci. 88 (2002) 1550–1555.
[23] C. Basavaraja, R. Pierson, D.S. Huh, a. Venkataraman, S. Basavaraja, Studies on properties of polyaniline-dodecylbenzene sulfonic acid composite films synthesized using different oxidants, Macromol. Res. 17 (2009) 609–615.
[24] G. Cravotto, P. Cintas, Sonication-assisted fabrication and post-synthetic modifications of graphene-like materials, Chem. Eur. J. 16 (2010) 5246–5259.
[25] A.C. Ferrari, Raman spectroscopy of graphene and graphite: disorder, electron–phonon coupling, doping and nonadiabatic effects, Solid State Commun. 143 (2007) 47–57.
[26] A. Das, B. Chakraborty, A.K. Sood, Raman spectroscopy of graphene on different substrates and influence of defects, Bull. Mater. Sci. 31 (2008) 579–584.
[27] D. Graf, F. Molitor, K. Ensslin, C. Stampfer, C. a Jungen, Hierold, et al., Spatially resolved Raman spectroscopy of single- and few-layer graphene, Nano Lett. 7 (2007) 238–242.
[28] Z.H. Ni, H.M. Wang, J. Kasim, H.M. Fan, T. Yu, Y.H. Wu, et al., Graphene thickness determination using reflection and contrast spectroscopy, Nano Lett. 7 (2007) 2758–2763.
[29] A. Jorio, E.H.M. Ferreira, L.G. Cançado, C.A. Achete, R.B. Capaz, Measuring disorder in graphene with Raman spectroscopy, in: S. Mikhailov (Ed.), Physics and Applications of Graphene – Experiments, InTech, 2011, pp. 439–454.
[30] C. Xiu-Yun, Graphene-like nanosheets synthesized by natural flaky graphite in Shandong, China, Int. Nano Lett. 3 (2013) 1–6.
[31] G. Wang, X. Shen, B. Wang, J. Yao, J. Park, Synthesis and characterisation of hydrophilic and organophilic graphene nanosheets, Carbon 47 (2009) 1359–1364.
[32] K.-S. Kim, S.-J. Park, Synthesis of carbon-coated graphene electrodes and their electrochemical performance, Electrochim. Acta. 56 (2011) 6547–6553.
[33] Y. Zhou, Z.-Y. Qin, L. Li, Y. Zhang, Y.-L. Wei, L.-F. Wang, et al., Polyaniline/multi-walled carbon nanotube composites with core–shell structures as supercapacitor electrode materials, Electrochim. Acta. 55 (2010) 3904–3908.
[34] L.M. Viculis, J.J. Mack, O.M. Mayer, H.T. Hahn, R.B. Kaner, Intercalation and exfoliation routes to graphite nanoplatelets, J. Mater. Chem. 15 (2005) 974.

[35] G. Wang, J. Yang, J. Park, X. Gou, B. Wang, H. Liu, et al., Facile synthesis and characterization of graphene nanosheets, J. Phys. Chem. C 112 (2008) 8192–8195.
[36] M.C. Arenas, E. Andablo, V.M. Castaño, Synthesis of conducting polyaniline nanofibers from single and binary dopant agents, J. Nanosci. Nanotechnol. 10 (2010) 549–554.
[37] T. Hino, T. Namiki, N. Kuramoto, Synthesis and characterization of novel conducting composites of polyaniline prepared in the presence of sodium dodecylsulfonate and several water soluble polymers, Synth. Met. 156 (2006) 1327–1332.
[38] X.S. Du, M. Xiao, Y.Z. Meng, Facile synthesis of highly conductive polyaniline/graphite nanocomposites, Eur. Polym. J. 40 (2004) 1489–1493.
[39] T. Kuilla, S. Bhadra, D. Yao, N.H. Kim, S. Bose, J.H. Lee, Recent advances in graphene based polymer composites, Prog. Polym. Sci. 35 (2010) 1350–1375.
[40] C. Xiang, L. Li, S. Jin, B. Zhang, H. Qian, G. Tong, Expanded graphite/polyaniline electrical conducting composites: synthesis, conductive and dielectric properties, Mater. Lett. 64 (2010) 1313–1315.
[41] F.R. Simões, L.O.S. Bulhões, E.C. Pereira, Synthesis and characterization of conducting composites of polyaniline and carbon black with high thermal stability, Polim. Cienc. Tecnol. 19 (2009) 54–57.
[42] Z. Mo, D. Zuo, H. Chen, Y. Sun, P. Zhang, Synthesis of graphite nanosheets/AgCl/polypyrrole composites via two-step inverse microemulsion method, Eur. Polym. J. 43 (2007) 300–306.
[43] S.E. Bourdo, T. Viswanathan, Graphite/polyaniline (GP) composites: synthesis and characterization, Carbon 43 (2005) 2983–2988.
[44] S. Bourdo, Z. Li, A.S. Biris, F. Watanabe, T. Viswanathan, I. Pavel, Structural, electrical, and thermal behavior of graphite–polyaniline composites with increased crystallinity, Adv. Funct. Mater. 18 (2008) 432–440.
[45] W. Feng, X.D. Bai, Y.Q. Lian, J. Liang, X.G. Wang, K. Yoshino, Well-aligned polyaniline/carbon-nanotube composite films grown by in-situ aniline polymerization, Carbon 41 (2003) 1551–1557.
[46] C. Harish, V.S. Sreeharsha, C. Santhosh, R. Ramachandran, M. Saranya, T.M. Vanchinathan, et al., Synthesis of polyaniline/graphene nanocomposites and its optical, electrical and electrochemical properties, Adv. Sci. Eng. Med. 5 (2013) 140–148.
[47] S.G. Vaidya, S. Rastogi, A. Aguirre, Surfactant assisted processable organic nanocomposite dispersions of polyaniline-single wall carbon nanotubes, Synth. Met. 160 (2010) 134–138.
[48] X. Huang, Z. Zeng, Z. Fan, J. Liu, H. Zhang, Graphene-based electrodes, Adv. Mater. 24 (2012) 5979–6004.
[49] H. Gómez, M.K. Ram, F. Alvi, P. Villalba, E. Lee Stefanakos, A. Kumar, Graphene-conducting polymer nanocomposite as novel electrode for supercapacitors, J. Power Sources 196 (2011) 4102–4108.